Fjord circulation induced by melting icebergs

Kenneth G. Hughes[1]

[1]College of Earth, Ocean, and Atmospheric Sciences, Oregon State University, Oregon, USA

Correspondence: Kenneth Hughes (kenneth.hughes@oregonstate.edu)

Abstract. TEXT

1 Introduction

Rivers of meltwater discharge from the base of glaciers in Greenland at rates of tens to hundreds of cubic meters per second. This fresh, buoyant water rises as a plume hundreds of meters up the face of the glacier, entraining many times more ambient seawater as it goes. If the discharge is high or the water column stratification weak, the plume reaches the surface and transitions to a down-fjord, surface current. Otherwise, the plume reaches neutral buoyancy and flows out at mid-depth. Either way, typical outflow speeds are $\mathcal{O}(10)\,\mathrm{cm\,s^{-1}}$ (e.g., Bendtsen et al., 2015; Jackson et al., 2022). This induces thicker, slower flows at depth to compensate. Over a summer, this plume-driven circulation is often enough to renew waters in the fjord (e.g., Gladish et al., 2015; Slater et al., 2022). Glacier melt can also induce circulation, but it is an order of magnitude weaker (Sciascia et al., 2013; Cowton et al., 2015).

If subglacial discharge is known, other quantities can be predicted. Slater et al. (2016), for example, uses buoyant plume theory to show that for a given subglacial discharge rate Q_{sg} in a salinity-stratified system with buoyancy frequency N, plume volume flux (and hence outflow) is proportional as $Q_{\mathrm{sg}}^{3/4}/N^{5/8}$ (see their Eq. 15). Glacier melt induced by a single plume scales as $Q_{\mathrm{sg}}^{1/3}$ or $Q_{\mathrm{sg}}^{2/5}$ depending on the details (Jenkins, 2011; Cowton et al., 2015). A corollary of these sublinear dependencies on Q_{sg} is that the same total discharge will lead to larger total volume fluxes and melting if the discharge is distributed among multiple plumes (Slater et al., 2015; Carroll et al., 2015) or over a longer melt season (Cowton et al., 2015).

These simple scalings provide the building blocks for more elaborate theories or wider-ranging applications. Zhao et al. (2021) use subglacial discharge to predict well the magnitude of overturning and horizontal recirculation in idealized fjords across a range of fjord widths, sill heights, wind forcing, and stratifications. And Slater et al. (2022) applies plume models to more than 100 fjords around Greenland to estimate that a total of $20\,000\,\mathrm{m^3\,s^{-1}}$ of meltwater discharge gets amplified by a factor of $\sim$50 due to entrainment. That is, a freshwater flux that is initially small by oceanic standards gets amplified to something that is better described in the oceanographer's unit of Sverdrups.

Subglacial discharge is not the only significant source of cool freshwater in many Greenland fjords. Iceberg melt is another and 'nowhere in the sea could a melting iceberg be expected to have a more pronounced effect on its environment than in the enclosure of a fjord' (Gade, 1979). At any given time, Sermilik Fjord is home to $\mathcal{O}(10\,000)$ icebergs and, as a result, the annual-average freshwater flux from melting icebergs is comparable to or larger than subglacial discharge (Moon et al., 2018; Moyer et al., 2019; Rezvanbehbahani et al., 2020). But the influence of this distributed meltwater source is not clear. As Enderlin et al. (2016) note, 'studies of fjord circulation and feedbacks [...] have largely ignored the contribution of iceberg melt within the fjords as a driver of fjord circulation'.

There are currently two complementary lines of study that shed light on the effects that icebergs and their melt have on fjord dynamics: (i) detailed studies of flow and melt of a single iceberg and (ii) fjord-scale simulations with icebergs as subgrid-scale components.

Dye releases and surveys near 100-m scale icebergs show upwelling at $7\,\mathrm{cm\,s^{-1}}$ beside the ice and horizontal extents of meltwater traceable 500–1000 m away (Josberger and Neshyba, 1980; Yankovsky and Yashayaev, 2014). Laboratory experiments of 10-cm scale icebergs in horizontal flows show that increasing the current increases the melt rates if the flow is $\gtrsim 2\,\mathrm{cm\,s^{-1}}$; below this, melt rate is insensitive to speed (FitzMaurice et al., 2017; Hester et al., 2021). Together, these results imply that, in a fjord with many icebergs, the meltwater from individual icebergs will almost certainly merge and that this combined meltwater flux could have a positive feedback as alluded to earlier: increased melt leads to increased velocities that further increases the melt rate given its velocity dependence.

Need to be careful with whether icebergs melting in presence of stratification. I think Josberger at least are in unstratified water

Davison et al. (2020) developed a subgrid-scale iceberg parameterization and implemented into simulations of Sermilik Fjord with 500×500 m horizontal resolution. Their simulations incorporated $\sim$10 000 cuboid icebergs distributed among 1400 cells with many of these cells ($\sim$40%) housing a single iceberg and others ($\sim$10%) housing more than 10 icebergs. Melt of these icebergs—inferred from each grid cell's temperature, salinity, and depth—lead to a meltwater flux distributed in three dimensions. In absence of subglacial discharge, but an otherwise summertime scenario with surface waters at 4°C, they found that iceberg melt induces slow currents ($\lesssim 0.02\,\mathrm{m\,s^{-1}}$) over the top 200 m. Since this water did not flush through the system quickly, the cooling and freshening effects of icebergs were strong: up to 5°C and 0.7 psu. Adding in a large subglacial discharge of $1200\,\mathrm{m^3\,s^{-1}}$ increased flushing and thereby reduced these effects by a factor of five. Using the same iceberg parameterization in a simulation of Ilulissat Icefjord, **?** found that these cooling and freshening effects improved agreement between model and observation.

Here, we examine the roles of icebergs—thermodynamical and mechanical—on fjord dynamics by developing simulations akin to that of Davison et al. (2020) and **?**, but at 30–50$\times$ their horizontal resolution (albeit over shorter time and space scales). This enables us to zoom in and explicitly resolve flow in, around, and under icebergs. In essence, our aim is to combine facets of the detailed, single iceberg studies and the fjord-scale studies. This aim grew out of a prequel study (Hughes, 2022) highlighting the nontrivial behavior of stratified flow when it impinges on and traverses a field of icebergs, rather than a single iceberg. That study, however, lacked iceberg thermodynamics, a glacier, and a subglacial discharge plume. We now add these processes.

2 Model setup

Our model setup builds on that of Hughes (2022), which had a melange comprising thermodynamically-inactive icebergs in the center of an open channel and was forced by imposed velocities at the boundaries. Here, we increase the realism by adding a glacier as a boundary at one end of a fjord and using meltwater

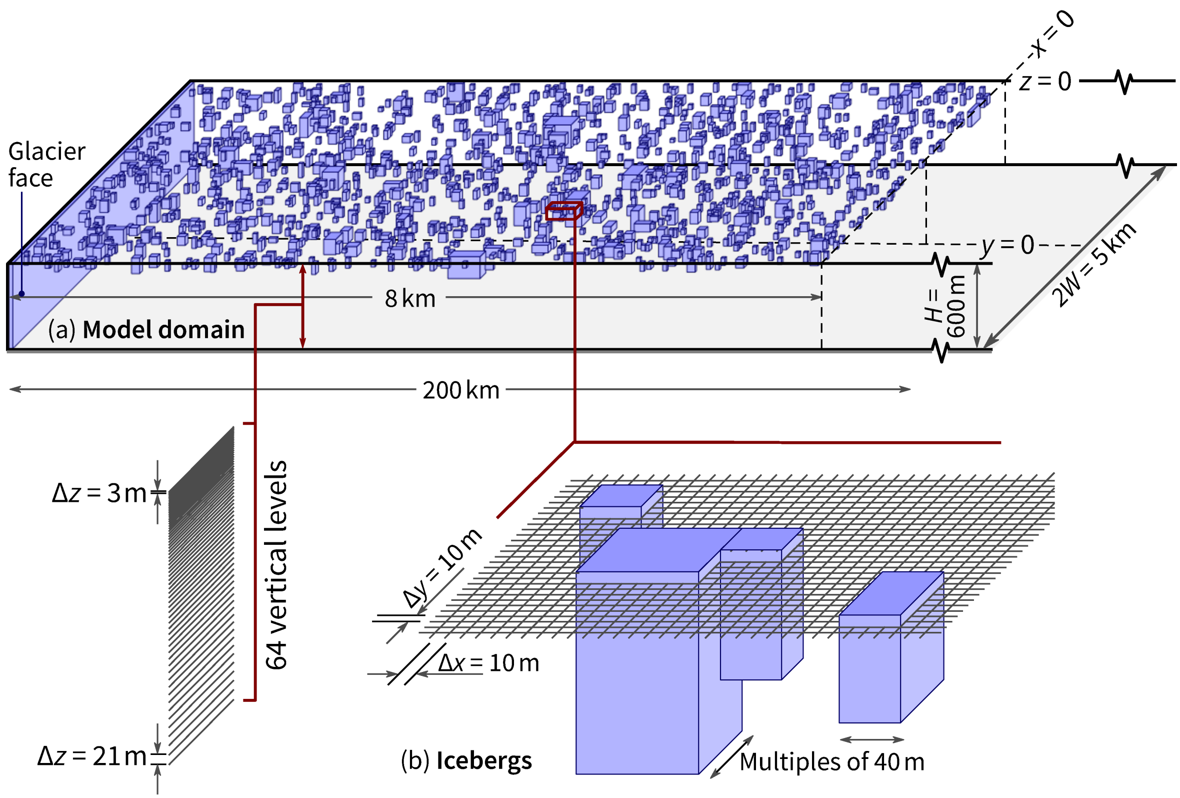

Figure 1. Model setup. In existing setup, I messed up and ended up with a glacier face at the far right end as well.

as the agent driving circulation, which is input through both melt at the ice–ocean interfaces and subglacial discharge.

Simulations are undertaken with the MITgcm (Marshall et al., 1997; Adcroft et al., 2004), in which it is possible to add volume-occupying ice cells at the surface (Losch, 2008) to serve as the icebergs.

2.1 Model domain

All simulations have a 3.8 km wide and $H = 600$ m deep fjord closed at one end by a glacier. The domain extends 100 km in the along-fjord (east–west) direction, but we focus on the first 4.5 km, which contains the melange (Figure 1a). Within this region, $\Delta x = \Delta y = 10$ m. Beyond this, Δx increases 3% per cell. There are 64 vertical levels, with the highest resolution of $\Delta z = 3$ m at the surface.

A time step of $\Delta t = 1$ s (sometimes 1.5 s) is used and simulations are run for 56 hours to allow a quasi steady state to develop for most cases (Appendix A). Unless otherwise noted, all results shown will be snapshots at the end of a simulation. Given this short simulation time (and lack of a sill), we are not addressing issues such as seasonality, deep basin circulation, or intermediary circulation (several-day-long baroclinic fluctuations driven at the fjord mouth).

For most simulations, the ambient water initially has a constant temperature and linear salinity stratification:

$$T_\mathrm{a}(z) = 2^\circ\mathrm{C} \tag{1}$$

$$S_\mathrm{a}(z) = 34.5 - 0.5z/H \tag{2}$$

Typical changes in these quantities by the end of the simulation are 0.02–0.1°C and 0.1–0.3 psu (Appendix A).

For cold waters like these, salinity has the dominant role on density; temperature then acts as a tracer (albeit not passive nor conserved). The 2°C value equates to approximately 4°C above the freezing, an average thermal forcing for Greenland fjords (Wood et al., 2021). The salinity increase $\Delta S = 0.5$ between the surface to the seafloor is lower than the more typical values of 2–4 observed in Greenland fjords (e.g., Straneo et al., 2011; Sciascia et al., 2013). We use the weak stratification and constant temperature for pedagogical reasons. Weak stratification lets the subglacial discharge plumes reach the surface, which induces a simple circulation regime: a single overturning cell. Constant temperature means that the effect of melting is always to cool water. If temperature varied with depth, then vertical advection induced by melting can lead to local warming at mid depths (Davison et al., 2022), thereby complicating our analysis. Sensitivity studies will use stronger salinity stratification or observed temperature and salinity profiles for initialization.

De Andrés et al. (2020) talks at length about role of stratification on plume neutral buoyancy

For $\Delta S = 0.5$, the mode-1 wave speed is approximately $c = 0.5\,\mathrm{m\,s^{-1}}$. With the Coriolis frequency set to $f = 1.37 \times 10^{-4}\,\mathrm{s^{-1}}$ (70°N), the internal Rossby radius c/f is approximately the same as the width of the fjord. If ΔS increases, so does the width of the fjord relative to the internal Rossby radius.

Will probably change 56 h to 48 h to be round number of 2 days. Most runs actually end at 32 h.

I'm going to redo all the runs on a larger domain. Will probably make the melange more like 7 or 8 km long and 5 km wide. I'll also play around with using shapes other than cuboids. Might also make default discharge 200 rather than 100 $m^3\,s^{-1}$

2.2 Melting icebergs

The icebergs making up the melange are cuboids with horizontal dimensions of multiples of 40 m (Figure 1c). Therefore, flow around individual icebergs is explicitly resolved, albeit coarsely. The size distribution of these icebergs follows from the power law given by (Sulak et al., 2017) for observations from Sermilik Fjord: the number of icebergs of a given horizontal area goes as $A^{-1.9}$. That is, smaller icebergs are more numerous than larger icebergs. Although larger ones often occur in reality, we impose a maximum iceberg size of 320×240 m. Most icebergs have a keel depth of 30–80 m. Further details and justification of the fixed cuboid approach are given by Hughes (2022).

The only way that the melange varies between simulations is in the number of icebergs within the region. We denote the fractional area of the sea surface covered by icebergs as λ. The example in Figure 1a has $\lambda = 0.1$, meaning that 10% of the sea surface is ice. At $x = 4.5$ km, this percentage drops abruptly to zero. This means that the melange has a sharp edge and helps us distinguish between the melange and non-melange regions.

Icebergs in our simulations input freshwater through subsurface melting but not through wave erosion or melting at the ice–air interface. Thermodynamics at all ice–ocean interfaces are treated with the three-equation formulation, and the same velocity-dependent turbulent transfer coefficients are used for the vertical sides and the basal face. Specifically, we adapt the ICEFRONT package implementation from Xu et al. (2012). Turbulent heat fluxes to the ice–ocean interface are

$$\text{heat transfer } [\mathrm{W\,m^{-2}}] = \rho c_\mathrm{p} \gamma_T |\mathbf{u}| \Delta T \tag{3}$$

$$\text{salt transfer } [\mathrm{m\,s^{-1}}] = \gamma_S |\mathbf{u}| \Delta S \tag{4}$$

where ΔT and ΔS are the difference between (i) the temperature and salinity in the ocean cells adjacent to ice and (ii) those at the ice–ocean interface. The transfer coefficients for heat and salt in units of $\mathrm{m\,s^{-1}}$

are $\gamma_T|\mathbf{u}|$ and $\gamma_S|\mathbf{u}|$ where

$$\gamma_T = 4.4 \times 10^{-3}, \tag{5}$$

$$\gamma_S = 1.24 \times 10^{-4}, \text{and} \tag{6}$$

$$|\mathbf{u}| = \min\left(\sqrt{u^2+v^2+w^2}, 0.04\,\mathrm{m\,s^{-1}}\right) \tag{7}$$

The values of γ_T and γ_S are far from well constrained; the significant figures are merely to help maintain a link to previous studies that used $\gamma_T = 1.1 \times 10^{-3}$ and $\gamma_S = 3.1 \times 10^{-5}$ (e.g., Xu et al., 2012; Sciascia et al., 2013). Observations suggest these values are too low at vertical or near-vertical ice faces in Greenland (Jackson et al., 2020; Schulz et al., 2022). We have increased γ_T and γ_S by a factor of four following the suggestion of Jackson et al. (2020, 2022) based on their scenario in which a resolved horizontal velocity is incorporated into the calculation of the transfer coefficients (rather than just vertical velocity). In our case, $|\mathbf{u}|$ values are calculated in the cells adjacent to ice–water interfaces. At each interface, two of the three velocity components will be nonzero; for example, $v \neq 0$ and $w \neq 0$ for an ice face in the y–z plane. The $0.04\,\mathrm{m\,s^{-1}}$ lower limit follows Slater et al. (2015) and is intending to represent unresolved melt-driven convection.

(Jackson et al. (2020) and some other studies define the conventional values of γ_T and γ_S in an alternate way. Namely, $\gamma_T = \sqrt{C_\mathrm{d}}\Gamma_T$ and $\gamma_S = \sqrt{C_\mathrm{d}}\Gamma_S$ where $C_\mathrm{d} = 2.5 \times 10^{-3}$, $\Gamma_T = 2.2 \times 10^{-2}$, and $\Gamma_S = 6.2 \times 10^{-4}$.)

I haven't yet increased default values by factor of four

Need to set transfer coefficients within plume

Do sensitivity study with Schulz parameterization?

2.3 Subglacial plume forcing

A single subglacial discharge plume issues from the grounding line in the center of the glacier (actually slightly off center to avoid a numerical instability.) Its dynamics are calculated using buoyant plume theory, which comprises a set of coupled ordinary differential equations in the vertical direction. At every time step, a steady state plume solution is found using the current temperature and salinity at the plume's location. This approach is typically treated in the MITgcm as a subgrid-scale parameterization (the ICEPLUME package; Cowton et al., 2015).

Need to move plume away from exact center

Here, a subglacial plume does not fit in a single cell, so we use the adapted approach of Zhao et al. (2022) in which the plume's entrainment and outflow is spread horizontally over a semi-circle (Figure 1b). Specifically, the extra mass flux is distributed over a 10-cell (100 m) radius, but weighted toward the center such that half the mass is added within a 5-cell radius. These horizontal scales roughly agree with the plumes observed at the surface at, say, Helheim Glacier (Melton et al., 2022). Vertically, outflow of the extra mass of fresher water is spread over five cells (or three or four if the plume reaches or nears the surface). Given the Δz is variable, the initial thickness of the outflowing layer depends on the plume's depth of neutral buoyancy. It will typically be 10–30 m, which is thin but comparable to the limited observations of near-field plume outflow (e.g., Jackson et al., 2017).

With 10 m horizontal resolution it is arguably possible to explicitly simulate a plume but this is computationally expensive in that it requires the model to be run nonhydrostatically, and the output is sensitive to the choice of viscosity and diffusivity (Xu et al., 2012; Sciascia et al., 2013; Slater et al., 2015; Gladish et al., 2015; De Andrés et al., 2018, e.g.). Since our focus is on the larger fjord dynamics, not the plume itself, we can avoid these challenges. We recognize, however, that we lose the ability to have a plume that overshoots its neutral buoyancy depth and then oscillates over the next $\sim$500 m as it travels down-fjord (Carroll et al., 2015). And no ability to generate internal waves? Cite Jesse's paper if it is accepted at some point.

Cowton et al. (2015) uses entrainment coefficient of $\alpha = 0.1$, but this gives a dilution rate of O(100), which seems to large. Need to look into this before rerunning models. Then again, Gladish et al. (2015) got amplification factor of 280...

I'm currently putting in plume at a temperature of 0C. Should really be using pressure-dependent freezing point, but this is pretty similar (-0.45C for freshwater at 600m)

2.4 Other model details

Vertical mixing is parameterized with the Klymak and Legg (2010) overturning scheme with a background viscosity and diffusivity of $A_\mathrm{v} = K_\mathrm{v} = 10^{-4}\,\mathrm{m^2\,s^{-1}}$. Horizontal viscosity is parameterized with a Smagorinksy viscosity with the `viscC2Smag` coefficient set to 2.5 together with a background value of

$A_\mathrm{h} = 10^{-3}\,\mathrm{m^2\,s^{-1}}$. Temperature and salinity are advected with a third-order flux limiter scheme (termed scheme 33 in the MITgcm).

Slater et al. (2018) and Hager et al. (2022) use 2.2 for Smagorinksy. Does this difference matter? Carroll et al. (2015) and Sciascia et al. (2013) use vertical viscosity of $10^{-3}\,\mathrm{m^2\,s^{-1}}$. But maybe I should use something smaller?

All model runs are hydrostatic, which are approximately four times faster than nonhydrostatic simulations for our set up. Need to do proper comparison between modes.

3 Results

3.1 Melt-driven circulation

Iceberg and glacier melt, by themselves, drive a weak overturning circulation (Figure 2). Maximum velocities of a few $\mathrm{cm\,s^{-1}}$ occur at the surface as the input of buoyant meltwater creates an along-fjord pressure gradient. Under the influence of Coriolis, and downstream of the melange, the fastest flows occur on the southern side of the fjord: the beginning of a coastal current appears at $x = 6\,\mathrm{km}$ in Figure 2a.

Within the melange, the fastest flows are on the northern side of the fjord. To understand this, consider a number of stationary icebergs melting into an unbounded region. In this case, meltwater would initially flow out in all directions and then, under Coriolis, evolve into clockwise eddy. This process would play out in manner similar to the buoyant meltwater plume next to a single iceberg (Yankovsky and Yashayaev, 2014) or, more generally, the Rossby adjustment of isolated lenses as described by Stuart et al. (2011). This tendency toward clockwise rotation is still evident in Figure 2b—note, for example, the surface inflow on the southern side—albeit modulated by the boundaries. (The Rossby adjustment of a cross-channel discontinuity in an open channel (Hermann et al., 1989) is instructive here. In that situation an asymmetric pattern arises with an eastward boundary current on the northern wall turning right—with some overshoot—and crossing the channel to become an boundary current on the southern wall. Much the same occurs here if we consider the end of the melange as the discontinuity.)

Meltwater input is significant at depths shallower than 100 m (Figure 2i), but not all of this flows outward. Instead, there is a net inflow below 50 m depth (Figure 2e). This inflow is necessary to make up for the divergence of vertical velocity at 50 m (Figure 3f), which is primarily caused by the depth-dependent input of meltwater (Figure 3g).

In the example in Figure 2, $\lambda = 0.1$ and there is $8 \times 10^6\,\mathrm{m}^2$ of ice in contact with water with a total meltwater input of $12\,\mathrm{m}^3\,\mathrm{s}^{-1}$. By comparison, Moon et al. (2018) estimate that in the first 20 km of Sermilik Fjord (the melange region), the input of iceberg melt is 60 and $200\,\mathrm{m}^3\,\mathrm{s}^{-1}$ for winter and summer, respectively. Hence, when scaled by a factor of approximately 4 to account for the shorter melange in our simulation, $12\,\mathrm{m}^3\,\mathrm{s}^{-1}$ is comparable to Moon et al.'s winter estimate.

Could also compare against latent heat of melting of 10^{12} W from Jackson and Straneo (2016)

3.2 Plume-driven circulation

Plume-driven flows are faster than iceberg-melt driven flows. For the example in Figure 3 with $Q_{\mathrm{sg}} = 100\,\mathrm{m}^3\,\mathrm{s}^{-1}$, surface currents away from the plume are $\mathcal{O}(10)\,\mathrm{cm\,s}^{-1}$ and have sufficient inertia to travel $\mathcal{O}(10)$ km before settling into a narrow coastal current. Closer to the glacier, an eddy forms. The structure of such eddies is sensitive to the fjord geometry and location of plume outflow (e.g., Carroll et al., 2017; Slater et al., 2018).

This plume-only run has a freshwater flux that is six times larger than the previously described iceberg-only run. However, this flux is flushed through the melange region ($x < 4.5$ km) more quickly and, consequently, the salinity deficit is only two times larger (compare Figs 2h and 3h). The temperature deficit is smaller in the plume run because adding cold water is less effective at cooling compared to extracting heat by melting ice. (Improve this explanation.)

3.3 How icebergs influence plume flow

Icebergs alter plume outflow in two clear ways: few larger eddies are replaced by many smaller eddies, and outflow is redistributed with depth.

Flow trajectories from the plume-only simulation in the previous section are shown in Figure 4 together with a simulation with both a plume and icebergs ($Q_{\mathrm{sg}} = 100\,\mathrm{m}^3\,\mathrm{s}^{-1}$ and $\lambda = 0.1$). The large eddy on the southern wall centered near $x = 3$ km does not arise when icebergs are present. This effect holds even when iceberg density is as low as $\lambda = 0.02$ (not shown). Evidently, the icebergs disrupt/introduce

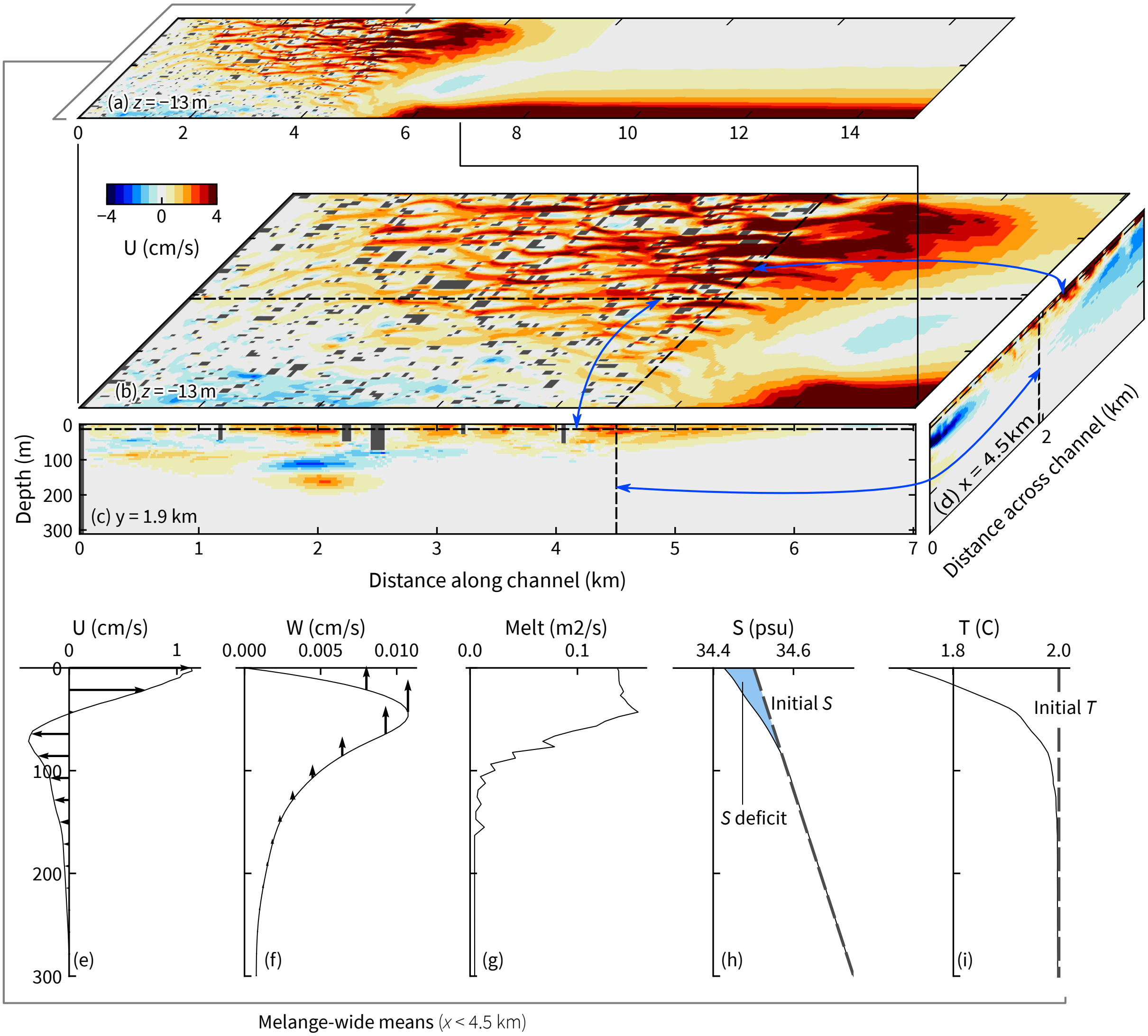

Figure 2. Dynamics driven only by ice meltwater as depicted in (a, b) plan view, (c) an along-fjord slice, and (d) a cross-fjord slice. The meltwater's tendency to circulate clockwise at the surface manifests as the stronger eastward velocities at the north end. Away from the melange, a buoyant coastal current forms, the start of which is visible at $x = 6$ km. At 50–200 m depth, mean flow within the melange region is westward (panel e). This inflow counteracts the divergence of the vertical flow (panel f), much of which is caused by rising meltwater. Cooling and freshening of water within the melange is concentrated in the top 100 m (panels g and h). This example has $\lambda = 0.1$. Add panel i label. Note that only top half is shown.

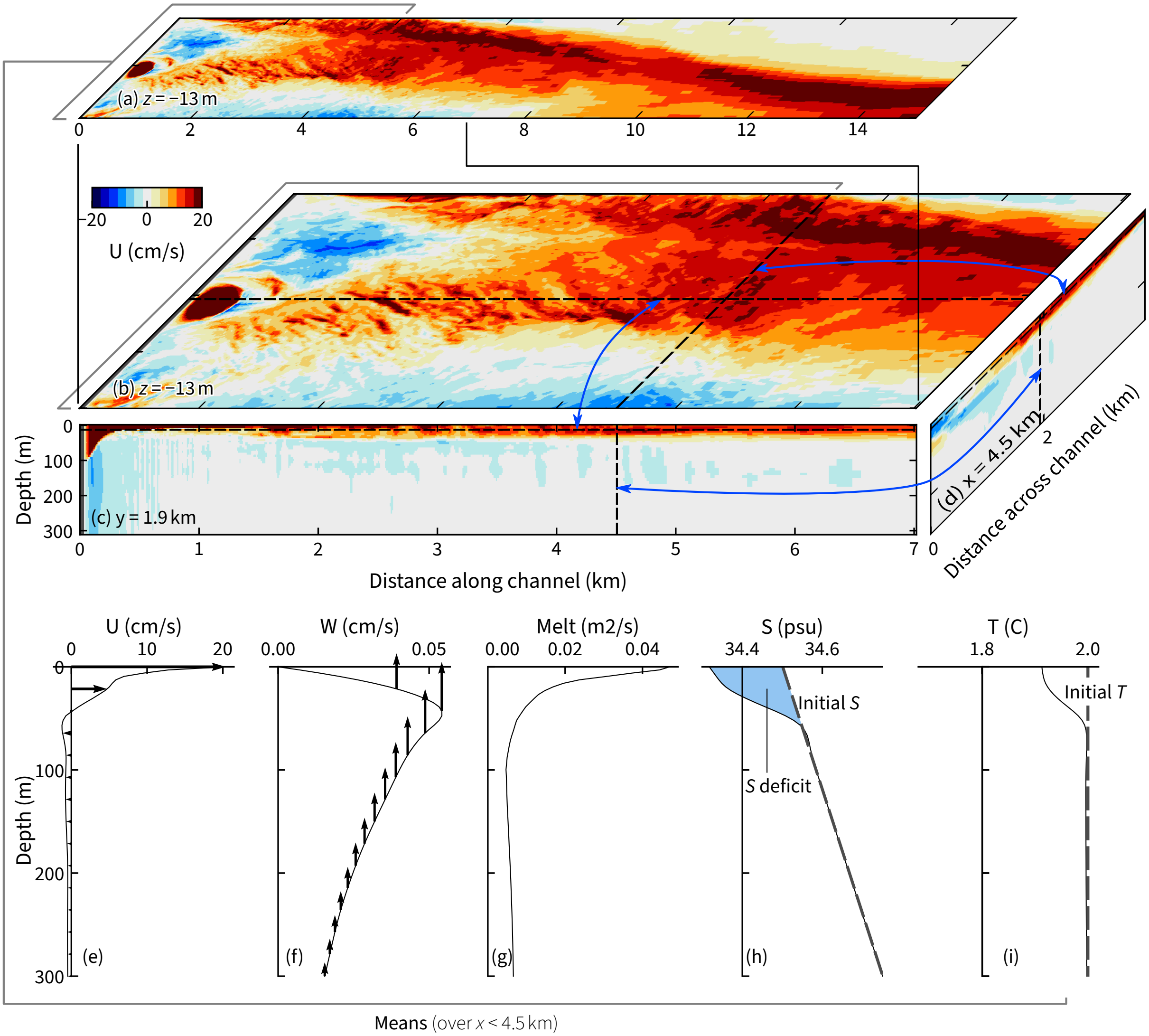

Figure 3. Dynamics driven by a subglacial discharge plume. (The only melting ice is the glacier). A surface jet and slow return flow (panel e) are caused by the average upward flow (panel f), which is dominated by the plume's vertical velocities of $\sim 1\,\mathrm{m\,s^{-1}}$. Cooler, fresher water is concentrated in the top 50 m. Note the different color scale and x limits compared to Figure 2. This example has $Q_{\mathrm{sg}} = 100\,\mathrm{m^3\,s^{-1}}$. Add panel h label. Match T and S limits to previous figure.

incoherency/something else... Figure out why and flesh out this argument. Instead of this large eddy, we see smaller ($\sim$100 m-scale) eddies behind most icebergs.

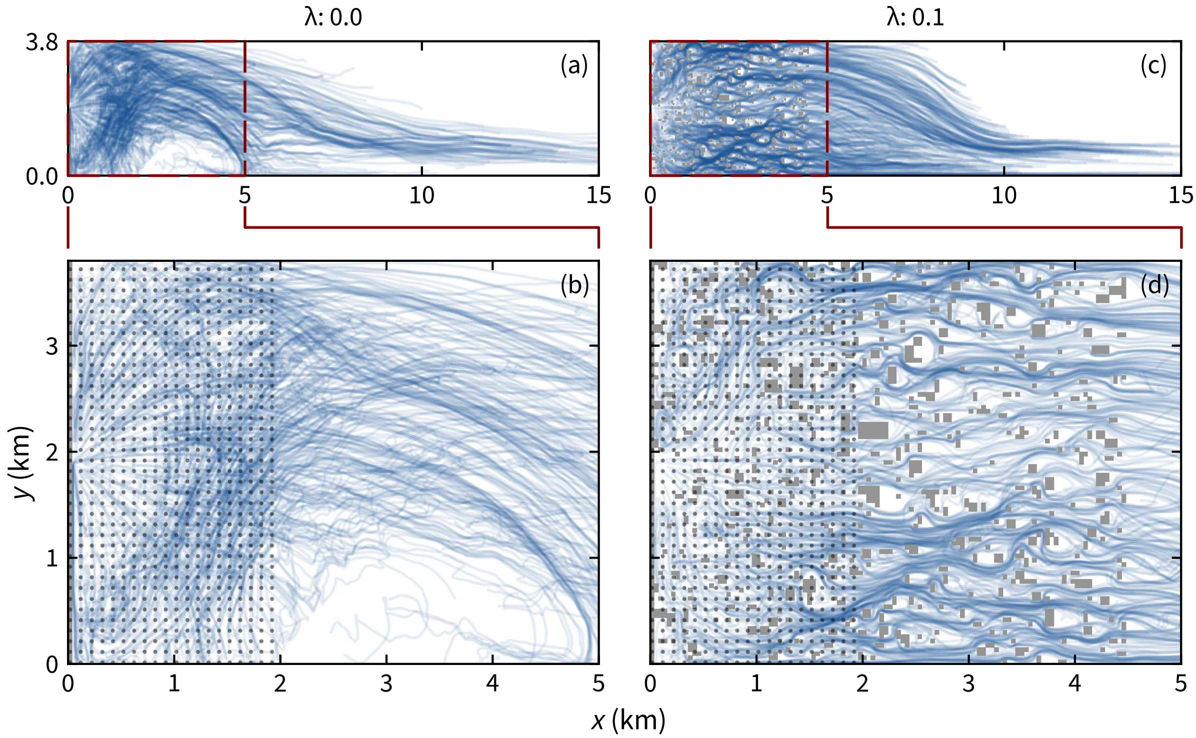

Figure 4. Surface circulation without and with icebergs. (a–b) Without icebergs, near-plume trajectories are in all directions; an eddy forms 2–4 km from the plume; and a coastal current forms beyond that. (c–d) With icebergs, the far-field circulation is similar, but the near-field circulation is ... The circulation shown is based on offline advection of the 760 evenly spaced particles for 24 hours based on the final (quasi steady) velocity field.

Each iceberg acts as a drag element and, together, they slow the plume outflow at the surface. For $Q_{\text{sg}} = 100\,\text{m}^3\,\text{s}^{-1}$ and without icebergs, the mean current speed in the top 20 m over $x < 4.5$ km is $15\,\text{cm}\,\text{s}^{-1}$ and the 95th percentile is $45\,\text{cm}\,\text{s}^{-1}$ (Figure 5). These speeds are approximately halved for $\lambda = 0.1$. Although the presence of icebergs introduces constrictions—which accelerate flow within—the maximum surface currents are, at best, only as fast as the average speed in the iceberg-free case.

Despite influencing current speeds, the number of icebergs has minimal influence on the overall outflow. We define Q_{out} as the cross-sectional flux of outflowing fluid:

$$Q_{\text{out}}(x) = \int\int u(x,y,z)|_{u>0}\,\mathrm{d}y\,\mathrm{d}z \tag{8}$$

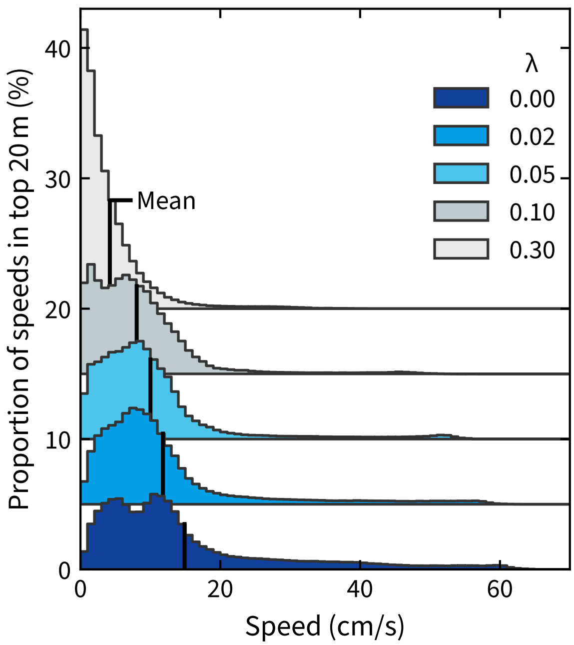

Figure 5. Near-surface flow velocities decrease as the number of icebergs increases. The velocity distribution comes from all grid cells within the melange region ($x < 4.5\,\text{km}$) in the top 20 m. Distributions are offset vertically for clarity. Add xtick marks for each baseline. Decide whether to include $\lambda = 0.2$, or note why not.

The net flux is Q_{sg}, but this net is the small difference of two much larger terms. For $Q_{\text{sg}} = 100\,\text{m}^3\,\text{s}^{-1}$, Q_{out} is two orders of magnitude larger (Figure 6c). Much of this increase happens as the plume is rising vertically and entraining ambient water (a process that is parameterized here with a one-dimensional plume model; Section 2.3). Entrainment continues, albeit more slowly, as the outflow moves down fjord and mixes vertically.

Since surface flows are reduced with increasing λ, but Q_{out} is comparatively constant, mid-depth flows must increase with λ. Within the melange, the fastest flows are not found at the surface once λ exceeds approximately 0.1 (Figure 6a). For $\lambda = 0.2$ and 0.3, outflow peaks at 60–70 m where there are fewer icebergs to impede motion. (Only a third of the icebergs in our setup extend down to these depths.) However, when the outflow passes the end of the melange, it becomes surface bound again regardless of its behavior beneath the melange (Figure 6b). To first order, the velocity structures are the same (including the cross-sectional structure; not shown).

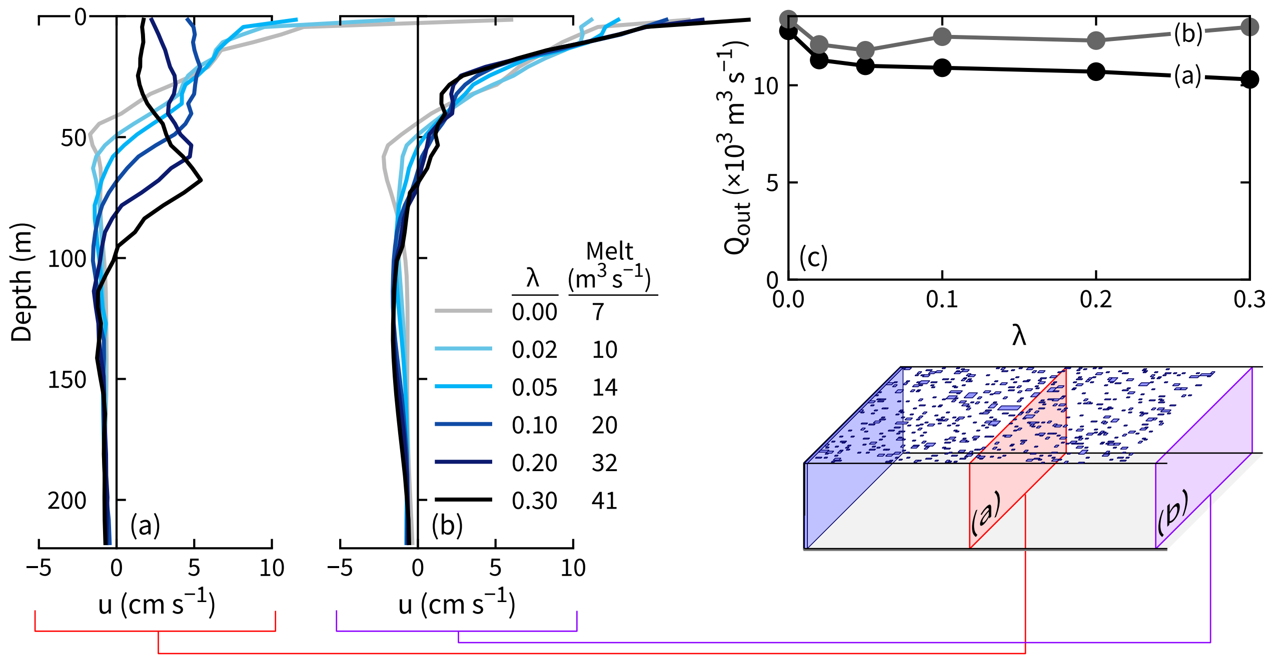

Figure 6. Among simulations with differing iceberg concentrations λ, differences in average cross-fjord velocity are (a) large within the melange but (b) small beyond the melange. (c) Regardless of location, overturning strength (Eq ?) is largely independent of λ. Only the top third of the domain is shown in panels a and b. These simulations all have $Q_{sg} = 100\,\mathrm{m^3\,s^{-1}}$. Check calculation of overturning strength within melange

Downstream of the melange, near-surface flow is easy to characterize as a geostrophic balance. The Coriolis and pressure gradient forces, both of which are large and nearly perpendicular to the fjord axis, cancel out (Figure 7).

One of Carroll et al. (2017)'s results was showing geostrophically balanced recirculation cells downstream of the glacier. Fraser et al. (2018) also noted that circulation is in geostrophic balance to a close approximation.

Within the melange, the pressure gradient and Coriolis terms are still the largest, but they are misaligned. The pressure gradient force—dominated by the sea surface height gradient $\nabla\eta$—has a significant component in the down-fjord direction. For $\lambda = 0.2$ as in Figure 7, $-\nabla\eta$ is $2\,\mathrm{mm\,km^{-1}}$ and is directed toward an angle of 50° from north. For simulations with more icebergs $-\nabla\eta$ gets larger and turns further

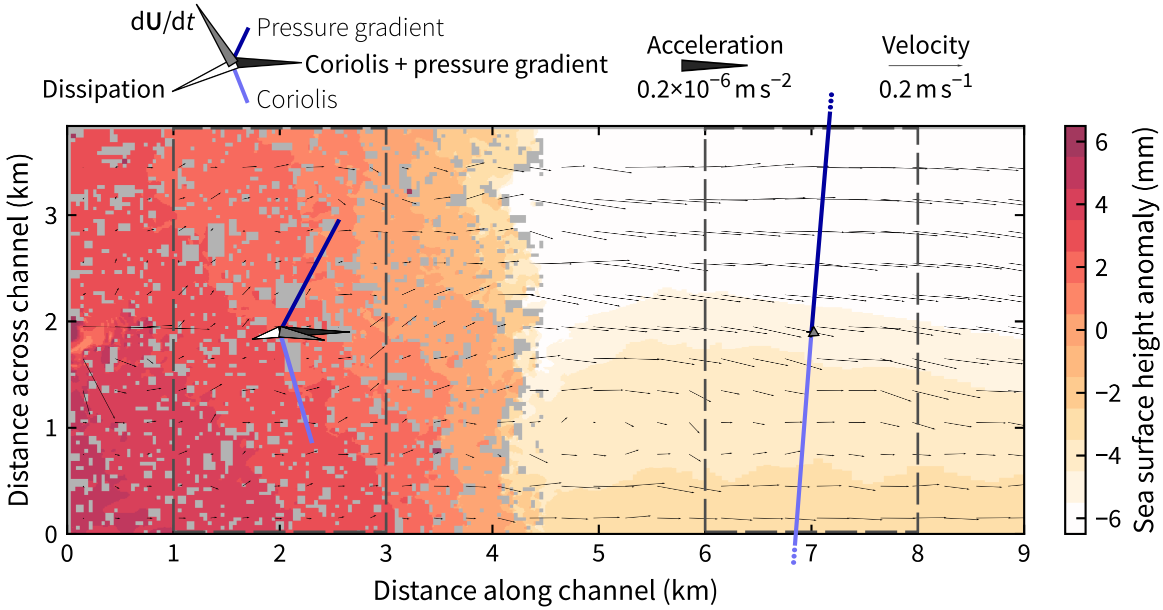

Figure 7. Large differences in the momentum budget inside and outside the melange for $\lambda = 0.2$. All quantities shown are averages over the top 20 m. Momentum budget terms are further averaged within the two dashed boxes.

down-fjord, and vice versa. With $\lambda = 0.05$, for example, $-\nabla\eta$ is $1\,\mathrm{mm\,km^{-1}}$ at an angle of 15° from north. More generally, $|\nabla\eta| \sim \lambda^{0.5}$.

The near-surface flow is not moving perpendicular to this gradient as would occur in geostrophic balance. Instead, its direction is closer to east-northeastward and consequently the Coriolis term has a positive component in the x direction.

Acting against these forces is viscous dissipation. In terms of being a momentum sink, the dissipative term is significant where there is vorticity injected as boundary layers separate. This occurs in the vicinity of each iceberg, and so within the melange, dissipation plays a first-order rule in the momentum budget.

The vector combination of the Coriolis, pressure gradient, and dissipative terms is aligned down-fjord. Therefore, fluid parcels accelerate down-fjord. Figure 7 shows this as the total acceleration:

$$\frac{\mathrm{d}\mathbf{u}}{\mathrm{d}t} = \frac{\partial \mathbf{u}}{\partial t} + (\mathbf{u}\cdot\nabla)\,\mathbf{u}, \tag{9}$$

but the acceleration is dominated by the advective term. Note, for example, how the flow leaving the control volume in Figure 7 at $x = 3$ km is faster than that entering at $x = 1$ km. At a fixed point the flow is approximately constant.

Make analogy to wind at earth's surface, which is ageostrophic due to friction.

4 Parameter space (working heading)

A lot of stuff about melt is slightly off since I wasn't including plume melt. For $Q_{\mathrm{sg}} = 100\,\mathrm{m^3\,s^{-1}}$, it adds about $2\,\mathrm{m^3\,s^{-1}}$ of melt

Thinking of doing another series of sensitivity tests with the minimum velocity value

The overturning circulation—with a thin, fast, surface outflow and a thick, slow outflow at depth—is dominated by the subglacial discharge plume. Meltwater coming from the icebergs has little effect, especially in the region down-fjord of the melange. At least, this is true for the subset of simulations in the previous section.

In the coming section, we test a wider parameter space to examine the influence of subglacial discharge, stratification, turbulent transfer at the ice–ocean interfaces, and the ambient water temperature. We focus on how these affect the outflow (evaluated just beyond the end of the melange) and the total ice melt rate.

Say something about default parameters

Say something about how much of simple plume scaling is already done in Slater et al. (2016) and probably elsewhere

To provide reference points for the magnitudes of Q_{out} as functions of the various parameters, we will include the values of the volume flux predicted using a simple half-conical plume model that has neither ice melt nor drag:

$$\frac{\mathrm{d}}{\mathrm{d}z}\left(r^2 w\right) = 2\alpha r w \tag{10}$$

$$\frac{\mathrm{d}}{\mathrm{d}z}\left(r^2 w^2\right) = g' r^2 \tag{11}$$

$$\frac{\mathrm{d}}{\mathrm{d}z}\left(r^2 w T_{\mathrm{p}}\right) = 2\alpha r w T_{\mathrm{a}}(z) \tag{12}$$

$$\frac{\mathrm{d}}{\mathrm{d}z}\left(r^2 w S_{\mathrm{p}}\right) = 2\alpha r w S_{\mathrm{a}}(z) \tag{13}$$

where r is the half-conical plume's radius and w its vertical velocity, T and S are temperature and salinity of the plume and ambient water (with subscripts p and a), g' is the plume's reduced gravity ($g\Delta\rho/\rho_0$), and $\alpha = 0.1$ is the same entrainment coefficient used in the full plume parameterization.

We solve Equations 10–13 numerically with initial conditions of $w_0 = 1\,\mathrm{m\,s^{-1}}$ and $r_0 = \sqrt{2Q_{\mathrm{sg}}/\pi w_0}$. The plume's volume flux is

$$Q_{\mathrm{p}} = \pi r^2 w/2 \tag{14}$$

where r and w are values when the plume either reaches the surface or neutral buoyancy. At this time, we assume the vertical volume flux turns 90° to become a horizontal volume flux.

Something about Sa, Ta are the same as the model initial conditions.

4.1 Role of iceberg density (λ)

To introduce Figure 8, we first revisit the simulations in which λ varies from 0 to 0.3 (Figure 8a). Compared against other parameters to be discussed, Q_{out} is insensitive to λ, and the simple plume model explains 80% of Q_{out}. This prediction is the λ-independent dashed line in Figure 8a. Loosely, this implies that the outflow's transit through and under the melange increases its magnitude by $\sim$20%. This increase occurs through the addition of meltwater and entrainment at the bottom of the outflow.

The total meltwater flux scales approximately linearly with λ. If we subtract the $4\,\mathrm{m^3\,s^{-1}}$ of melting at the glacier face, we find that $Q_{\mathrm{melt}} \propto \lambda^{0.90}$ and that $Q_{\mathrm{melt}} \propto A_{\mathrm{ice}}^{0.96}$ where A_{ice} is the total surface area of icebergs in contact with water. This scaling agrees with satellite(?) observations from Enderlin et al. (2018) who note that meltwater fluxes from icebergs can be reasonably approximately as a linear function of submerged ice area (Need to reread and check context of this statement).

4.2 Role of subglacial discharge (Q_{sg})

Subglacial discharge has a large, mostly predictable influence on outflow. For weaker discharge or stronger stratification, the plume reaches neutral buoyancy before the surface and $Q_{\mathrm{out}} \propto Q_{\mathrm{sg}}^n$ where $n \approx 0.75$ (e.g., Slater et al., 2016). For stronger discharge or weaker stratification, the plume reaches the surface and the exponent n is approximately 0.37. Say something about n being 0.37 rather than theoretical 0.33. For our default, relatively weak stratification of 0.5 psu/600 m, we are in the $Q_{\mathrm{sg}}^{1/3}$ regime whenever $Q_{\mathrm{sg}} \gtrsim 10\,\mathrm{m^3\,s^{-1}}$.

Mention also Figure 3 of Xu et al. (2013).

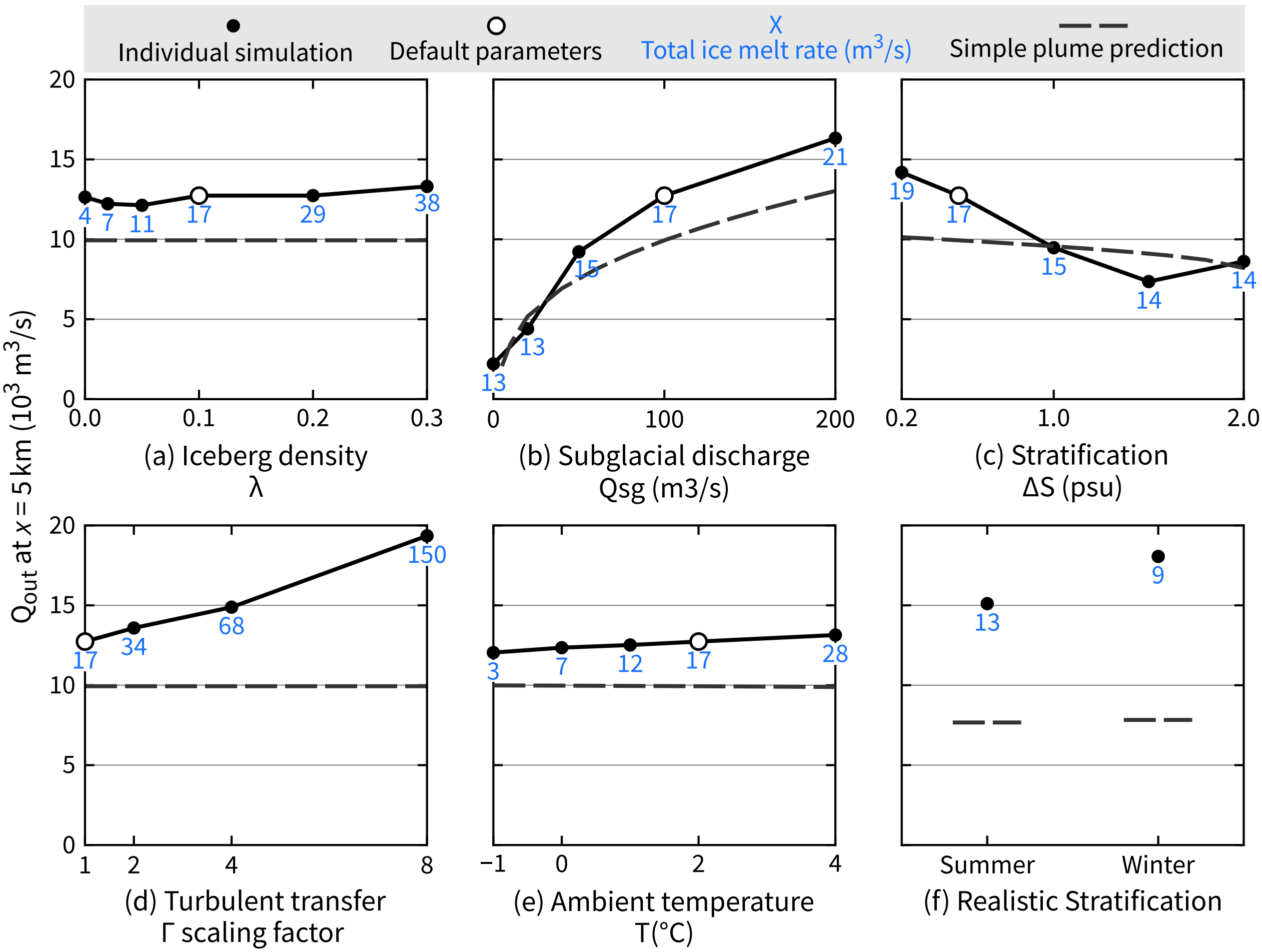

Figure 8. Outflow and ice melt is sensitive to some model parameters and insensitive to others. Panel a melt numbers don't match Figure 6 because I'm using different snapshots (I think). This will be fixed in future.

Except for the small discharge runs ($Q_{\mathrm{sg}} \leq 20\,\mathrm{m}^3\,\mathrm{s}^{-1}$), outflow is approximately 20% larger than predicted by the simple plume model—the same as for λ.

The total melt rate with no discharge is $13.4\,\mathrm{m}^3\,\mathrm{s}^{-1}$. This equates to an average melt rate of $11\,\mathrm{cm\,d}^{-1}$ water equivalent spread over the $10^7\,\mathrm{m}^2$ of ice ($\lambda = 0.1$). For all but 0.3% of this ice area, the current speed in the adjacent cell is below the $4\,\mathrm{cm\,s}^{-1}$ threshold (Equation 7). Hence, the total melt is controlled by the choice of this threshold that represents the effects of melt-driven convection.

I haven't calculated the above percentages exactly. I need to redo these and weight the average by the size of the ice-adjacent cells.

Remind reader somewhere that no-discharge simulation is shown in Figure 2

With increasing discharge, melt increases linearly. A fit across the five simulations from 0 to 200 $\mathrm{m^3\ s^{-1}}$ gives

$$Q_{\mathrm{melt}} = 13.4 + 0.04 Q_{\mathrm{sg}} \tag{15}$$

This is curiously similar to Figure 6 of Cenedese and Gatto (2016). Need to investigate further. By comparison, plume-driven melt at the glacier face is

$$Q_{\mathrm{melt}} = 0.4 Q_{\mathrm{sg}}^{0.38} \tag{16}$$

which is an order of magnitude smaller than Equation 15.

This is empirical for the specific salinity stratification. Elaborate on what this means.

Maybe also compare to melt $\propto Q_R^{0.32}$ from Jackson et al. (2022) and $Q^{1/3}$(?) in Jenkins (2011).

4.3 Role of salinity stratification ($\mathrm{d}S/\mathrm{d}z$)

Outflow typically weakens with increasing salinity stratification (Figure 8c). Qualitatively, this makes sense given the plume's behavior: with increased stratification, the plume tends toward neutral buoyancy earlier, which slows it down and causes it to entrain less ambient fluid overall. Less entrainment during the plume's rise equates to a weaker outflow. This argument, however, does not explain the $\sim$40% reduction in Q_{out} as ΔS goes from 0.2 to 2.0. The simple plume model predicts only a 20% reduction.

In weak stratifications in which the plume reaches the surface, the outflow passes through the melange and moves slowly but surely down fjord as, for example, in Figure 4d. Conversely, outflow has a different fate if the plume flows out before reaching the surface. Consider a case in which the plume reaches neutral buoyancy at $\sim$100 m, which leads to the outflow interacting with far fewer icebergs. As per the momentum budget analysis in Section 3.3, this implies that the plume flow will tend toward geostrophic balance. In this case, geostrophic balance manifests as an eddy in front of the glacier. In other words, the outflow at $x = 5$ km is reduced because much of the flow recirculated back up fjord before reaching this point.

Some of this is probably wrong and based on an instability when the plume is in the exact center of the domain.

4.4 Role of turbulent transfer coefficients (γ_T, γ_S)

Increasing the ice–ocean turbulent transfer coefficients increases melt rates and outflow. Doubling the transfer coefficients nearly doubles the input of meltwater, and similarly for quadrupling. For these two scaling factor, the extra meltwater induces 7 and 17% more outflow, respectively.

We see hints of a positive feedback when we further increase the transfer coefficients. That is, increased turbulent transfer coefficients lead to more melt, which increases the speed of the surface outflow, which increases the turbulent transfer through the dependence on speed (Equation 3). Specifically, using $8\times\gamma_{T,S}$ leads to $8.4\times$ the total melt.

This feedback is, of course, not large. Instead, to first order the melt rate should be considered linearly proportional to γ_T and γ_S. The reason for this proportionality is that turbulent transfers to the ice–ocean interface are velocity dependence only if speeds exceed $0.04\,\mathrm{m\,s^{-1}}$ (Equation 7). For $1\times, 2\times$, and $4\times\gamma_{T,S}$, only 24–26% of ice-adjacent cells exceed this threshold. For $8\times\gamma_{T,S}$, this goes up, but only to 31%.

4.5 Role of ambient temperature (T_a)

This section will change a bit once I get

Ambient temperature has approximately linear influences on both outflow and melt rate. The effect on outflow is incremental: a 1°C increase leads to a $< 2\%$ increase to the otherwise plume-driven outflow. The effect on melt rate, by comparison, is large. We find that total melt is proportional to $\Delta T^{1.1}$ where the thermal forcing $\Delta T = T - T_\mathrm{fp}$ with $T_\mathrm{fp} \approx -1.9$°C. If we consider only icebergs, the total melt scales as $\Delta T^{1.2}$.

These exponents of 1.1 and 1.2 are lower than might be expected. For a vertical ice face melting in a stratified environment without any discharge, Greisman (1979) predict that melt will scale as $\Delta T^{1.6}$, and this prediction agrees with 1-m resolution simulations of an idealized Store glacier by Xu et al. (2013). The found that melt scaled as $\Delta T^{1.61}$ for simulations without subglacial discharge. Magorrian and Wells (2016) even find a depth-averaged melt rate proportional to ΔT^2. (Need to check conditions under which this is valid. Might not apply here.)

4.6 Realistic temperature and salinity

Might be interesting to know if melt remains at depth due to near-surface pycnocline. And if we see more than a single overturning cell. Observations from some fjords show two inflow and two outflow layers (Inall et al., 2014; Mortensen et al., 2020), as do some models (Sciascia et al., 2013; Zhao, 2022).

These runs are also probably wrong on account of the instability with the plume in the middle. I therefore haven't written anything.

I should do the winter run without discharge

5 Comparison with a sub-grid scale iceberg parameterization

Resolving flow around icebergs is desirable, but bears a computational burden: simulating even a fraction of a fjord at 10-m resolution for a few days requires $\mathscr{O}(1000)$ CPU hours. This drops to $\mathscr{O}(0.1)$ CPU hours if we lower the resolution to, say, 400 m and parameterize (rather than resolve) icebergs. But does this entail a loss of accuracy?

No, the loss of accuracy is minimal, as we will show.

5.1 Setup of coarse simulations

We rerun the same 22(?) simulations described in Section 4 at 400-m horizontal resolution with the Davison et al. (2020, 2022) iceberg scheme. Hereafter, we will refer to the original 10-m grid as the *fine grid* and this new 400-m grid as the *coarse grid*.

The iceberg populations and dimensions are the same between the two grids. For the default value of $\lambda = 0.1$, a typical 400×400 m cell contains 3–5 icebergs. As for the fine grid, icebergs in the coarse simulations are stationary, and the same ice–ocean interface thermodynamics and turbulent transfer coefficients are used (see Section 2.2).

For the coarse grid, the subglacial plume fits within one cell, so no smoothing is used as it was for the fine grid (Section 2.3). Horizontal and vertical mixing schemes are the same between the different grids.

Do I want to say this this last point is probably a bad idea? But that it's a second-order effect, I think?

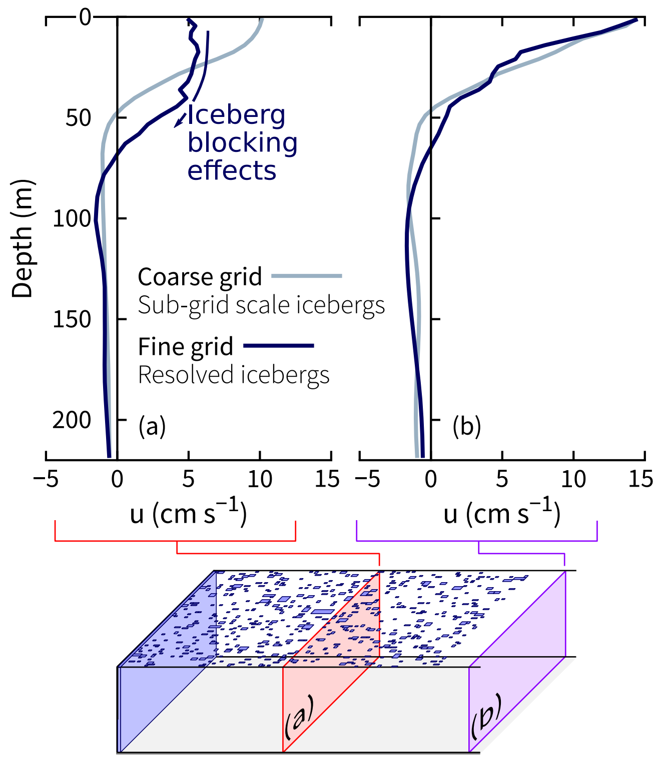

Figure 9. Comparing velocity profiles within and beyond the melange using two different approaches to simulating iceberg dynamics. Both models have the same population of icebergs. In the coarse-grid simulation, icebergs are sub-grid scale components. In the fine-grid simulation, icebergs are explicitly resolved and occupy volume. The two simulations use the default parameters ($\lambda = 0.1, Q_{sg} = 100\,\mathrm{m}^3\,\mathrm{s}^{-1}$).

5.2 Coarse vs fine simulations

Icebergs induce a blocking effect and thicken the outflow. Figure 6, for example, shows the outflow in the absence of icebergs as a 20-m thick surface-intensified jet, but with many icebergs it becomes thicker, slower, and peaks at $\sim 50\,\mathrm{m}$ depth. Beyond the melange, the blocking effect disappears and the jet becomes surface intensified.

The blocking effect does not occur when using the Davison et al. (2020) iceberg scheme. Instead, we see surface-intensified jets within the melange (Figure 9a) as well as beyond the melange (Figure 9b). Surface flows within the melange in the coarse simulations are up to two times too fast compared to the fine grid.

Davison et al. (2020) recognized that the icebergs act as barriers: one input to their scheme is a three-dimensional array that dictates the fraction of each grid cell occupied by ice. In principle, seawater should be squeezed through the remaining fractions of the cells. Our inspection and tests of the code, however, showed that the iceberg barrier mask is not implemented correctly and has no effect.

Check out testing of this hypothesis in idealised/iceberg_check_barrier_effect and idealised/melange_vs_iceberg_column

The lack of a blocking effect is not a major concern if we are interested in flow properties beyond the melange. Figure 9b shows that the average cross-channel velocity profiles just 500 m downstream of the melange agree reasonably well between the coarse and fine grids, as do the temperature and salinity (not shown). More generally, there is reasonable agreement between coarse and fine simulations across the 22 scenarios. The average discrepancy in outflow evaluated just down-fjord of the melange is less than 10% (Figure 10a). Similarly, the average discrepancy in total melt rate is less than 25% (Figure 10b).

These percentages definitely need to be recalculated correctly.

Given these good agreements, we recommend using the Davison et al. iceberg scheme for fjord-scale or larger models unless there is a specific goal to simulate vertical profiles of mass and freshwater fluxes. If not, then the iceberg scheme is sufficient to predict realistic fjord-wide distributions of sinks of heat and salt from melting icebergs—at least to within the known limitations of the turbulent transfer coefficients (see Section ?)

6 Discussion

Notes in no particular order

Jackson et al. (2020) shows that to get melt rates correct at LeConte, you could increase the drag coefficient by 175. Or, you could use much more modest increases of 4x(?) if you include the observed velocity of $0.2\,\mathrm{m\,s^{-1}}$. The implication then is that you want to understand the velocity in the vicinity of ice. Slater et al. (2018) showed how the circulation would double the melt of the glacier in Sarqardleq Fjord. They found ...

I'm not resolving the ambient melt plumes at the interface of the icebergs. These plumes will entrain water and thereby increase their outflow. The model is therefore likely underestimating how much of an

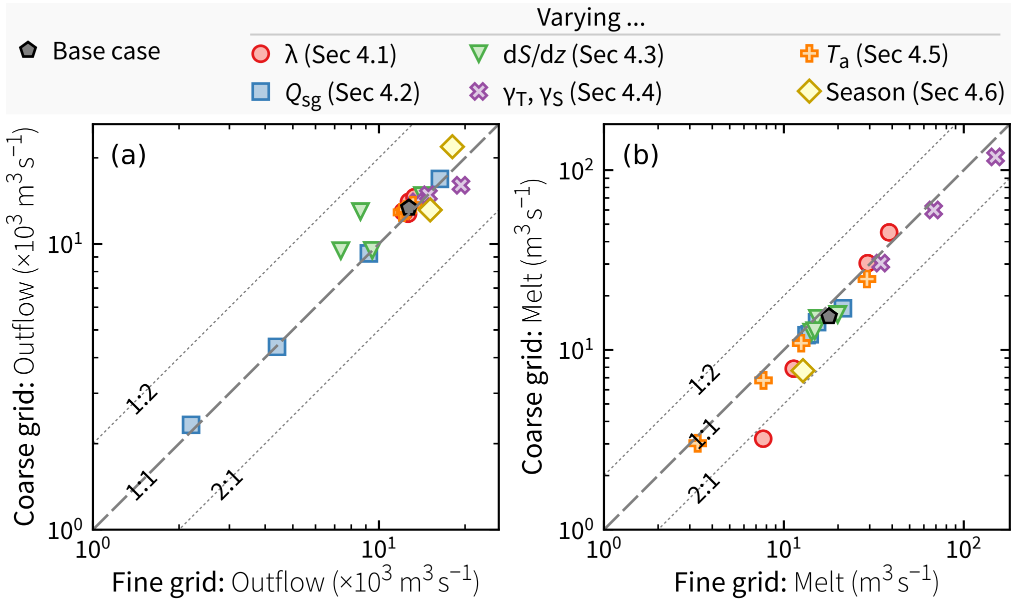

Figure 10. Coarse and fine grid simulations agree well in terms of (a) outflow and (b) meltwater flux. The coarse-grid simulations use the sub-grid scale iceberg parameterization from Davison et al. (2020) and are 40× coarser in the horizontal (400 m vs 10 m) than the fine-grid simulations described in the rest of the paper. Neither melt is calculated correctly. They'll both be higher than the values here.

effect icebergs have. At the same time, these ambient plumes don't rise up far before reaching neutral buoyancy. So there is a series of weak intrusions than extend only a few hundred meters (Jackson et al., 2020) rather than a few larger plumes. What do papers like Magorrian and Wells (2016) have to say about this?

My results showed that the 0.04 m s^{-1} threshold used to approximate the effect of ambient plumes plays a large role. This is more reason to get this ambient melt problem solved. Hager et al. (2022) set threshold to 0.9 for summer and 0.1 m s^{-1} in winter. Josberger and Neshyba (1980) measured vertical velocities of 0.07 m s^{-1} next to iceberg off Canada.

Also, I've yet to touch on the issue of how turbulent transfer coefficients should depend on model resolution. Sciascia et al. (2013), for example, found that changing resolution from 10 to 50 m reduced mean glacier melt rate by factor of 2, but that increasing to 5 m also lead to decrease in melt rate. Overall, 10 m gave highest rate out of 5, 10, 20, and 50 m. Xu et al. (2012) found ∼60% higher melt rates with horizontal resolution of 2 m instead of 20 m. Slater et al. (2015) found 15% decrease in melt moving from 5 to 10 m. Maybe finite-element models are the answer, or at least a complementary approach (e.g. Kopera et al., 2022). According to Shin et al. (2021), you need 24 grid points per cube to resolve turbulent features at the edges of cubes.

As Malyarenko et al. (2020) put it, ‘external velocity sources can significantly complicate the entrainment rate and the boundary layer structure next to the sloping interface’. The complex pathways through the melange can be thought of as something affecting the "external velocity sources"

I haven’t dealt with forcing coming in from mouth of fjord, which would increase velocity variance.

Truffer and Motyka (2016) Section 5.3 notes that melange may well be blocking ascent of the plume. Although my model isn’t sufficient to prove that this blocking can occur, it does show that the plume prefers to flow out beneath the melange. Truffer and Motyka (2016) also point out that ‘much speculation remains ... about the behavior and impact of submarine melting on the melange’. Also relevant to this point is **?**

Is it possible to use measured rates of melting across the melange from Enderlin to tune turbulent transfer coefficients? It’s hard to tune coefficients at the glacier face because it’s hard to accurately measure it’s melt rate. Maybe it’s easier to use icebergs, which are floating and don’t have an upstream source like a glacier does. In other words, the mass budget is easier.

Can I compare results to Hester et al. (2021) who looked at melting of one iceberg in a current vs not in a current.

What is depth distribution of meltwater among the simulations? As Moon et al. (2018) notes, large-scale models often simply add freshwater to surface. And does this have any implications for the work of Slater et al. (2022), who note that role of icebergs is missing

How does glacial meltwater fraction vary with distance down fjord? How does this compare to observations by Mortensen et al. (2020)?

Does plume thickness/melting agree at all with Everett et al. (2021)?

Obvious next step would be to introduce intermediary circulation a la Gladish et al. (2015). Feasible to look at that time scale and see what happens to the wave. Though not immediately obvious how to do it in 3D

7 Conclusions

Code availability. TEXT

Data availability. TEXT

Appendix A: Spin up

All simulations start from rest with horizontally homogeneous temperature and salinity. Plume-induced currents spread radially over the a few hours until reaching the fjord boundaries and then continue extending down-fjord thereafter. For the base case, currents reach the eastern end of the melange within 12 h (Figure A1). Currents speeds at this location averaged across the fjord keep increasing until $t \approx 24$ hr after which they are in an approximately steady state (solid line in Figure A2a). Temperature at the same location continues to drop at $t = 24$ h, which is to be expected given the distributed heat sink that is the melange. After 48 h, the rate of change of temperature is small (solid line in Figure A2b) because the heat loss from ice is largely balanced by a down-fjord flux of cooler water.

For the plume-only case, there are no icebergs acting as obstacles for the outflowing plume, so it is quick to reach an energetically steady state. There is cooling due to the input of subglacial discharge, but it is more gradual than in simulations with icebergs.

For the ice-only case, a steady state is not reached before the simulation ends. Currents keep increasing and temperatures keep decreasing as ice melts. Based on a coarse grid simulation (Section 5), we estimate that this particular scenario requires $\sim$100 h for current speed to reach a steady value, but temperatures continue to drop at a nearly constant rate of $\sim$0.03°C d^{-1} because the down-fjord flux of cool water is too weak to balance the heat lost to melting.

Need to explain Figure A2c

Say something about wanting to evaluate models all at same time, rather than each one's steady state. Maybe put this not in section 2.

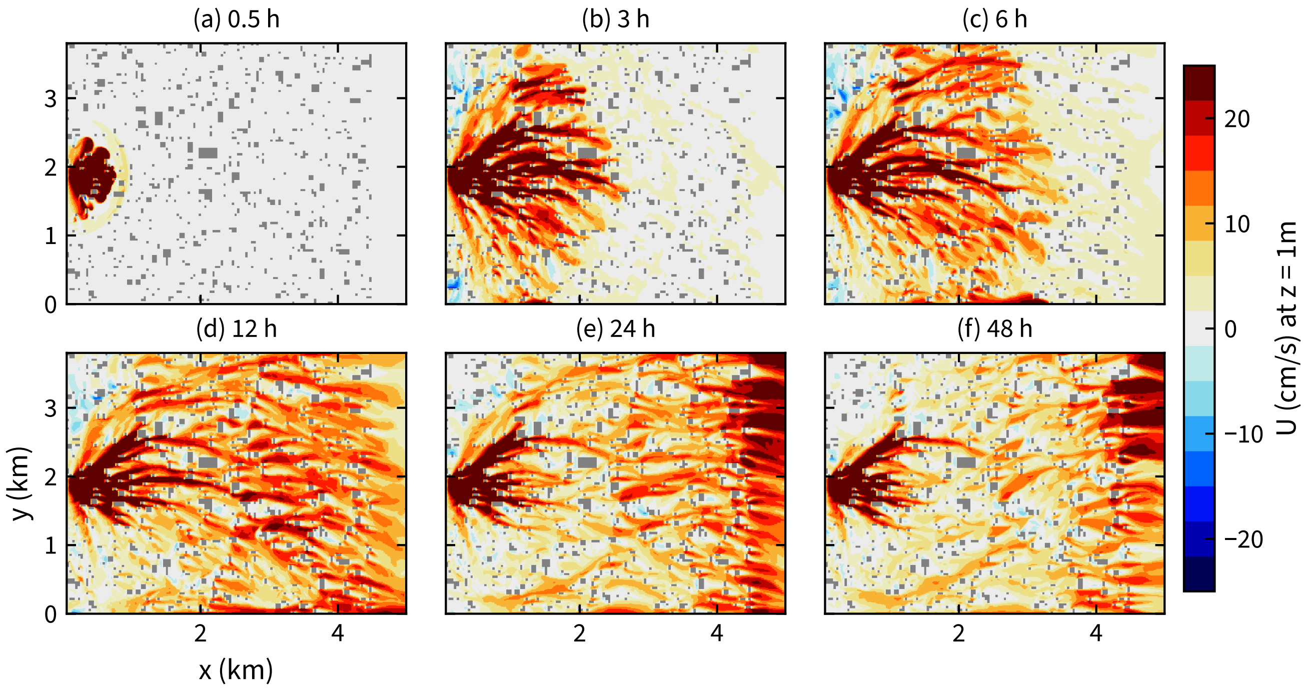

Figure A1. Spin up of the surface velocity field for $\lambda = 0.1$, $Q_{\mathrm{sg}} = 100\,\mathrm{m^3\,s^{-1}}$. Should change the limits to show that, outside the melange, things aren't steady.

A1

Author contributions. TEXT

Competing interests. TEXT

Disclaimer. TEXT

Acknowledgements. TEXT

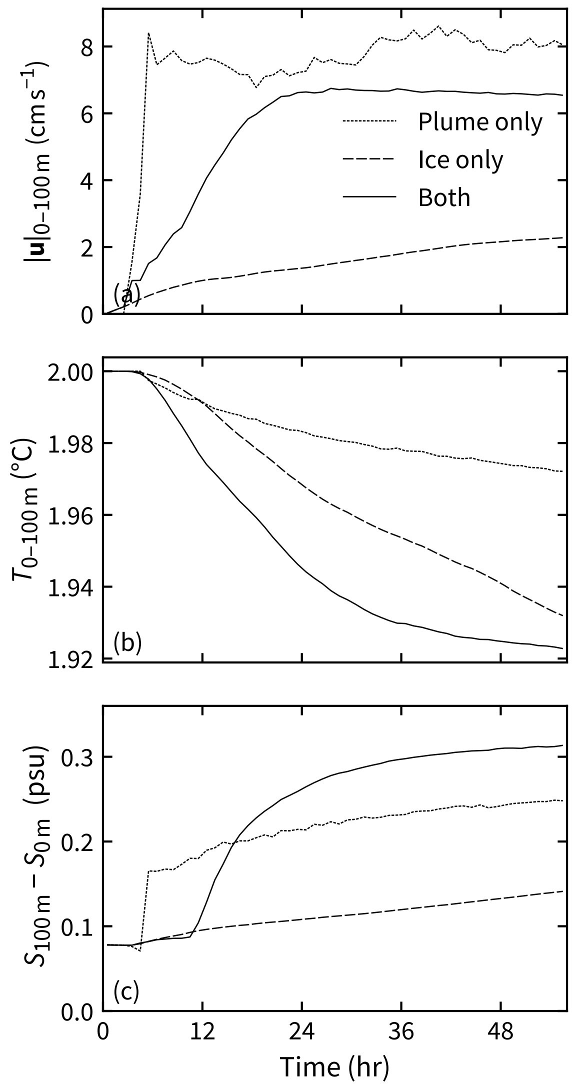

Figure A2. Simulations tend toward steady state within 48 hours, except for the less energetic ice-only case. (a) The quantity $\sqrt{u^2+v^2+w^2}$ averaged over the top 100 m of a cross section at the eastern end of the melange ($x = 4.6$ km). (b) As for panel a but for temperature. (c) The salinity difference at the same location. Caption could be much improved.

References

Adcroft, A., C. Hill, J.-M. Campin, J. Marshall and P. Heimbach (2004), Overview of the formulation and numerics of the MIT GCM, in *Proceedings of the ECMWF seminar series on Numerical Methods, Recent developments in numerical methods for atmosphere and ocean modelling*, pp. 139–149.

Bendtsen, J., J. Mortensen and S. Rysgaard (2015), Modelling subglacial discharge and its influence on ocean heat transport in Arctic fjords, *Ocean Dyn.*, 65, 1535–1546, https://doi.org/10.1007/s10236-015-0883-1.

Carroll, D., D. A. Sutherland, E. L. Shroyer, J. D. Nash, G. A. Catania and L. A. Stearns (2015), Modeling turbulent subglacial meltwater plumes: Implications for fjord-scale buoyancy-driven circulation, *J. Phys. Oceanogr.*, 45, 2169–2185, https://doi.org/10.1175/JPO-D-15-0033.1.

Carroll, D., D. A. Sutherland, E. L. Shroyer, J. D. Nash, G. A. Catania and L. A. Stearns (2017), Subglacial discharge-driven renewal of tidewater glacier fjords, *J. Geophys. Res. Oceans*, 122, 6611–6629, https://doi.org/10.1002/2017JC012962.

Cenedese, C. and V. M. Gatto (2016), Impact of a localized source of subglacial discharge on the heat flux and submarine melting of a tidewater glacier: A laboratory study, *J. Phys. Oceanogr.*, 46, 3155–3163, https://doi.org/10.1175/JPO-D-16-0123.1.

Cowton, T., D. Slater, A. Sole, D. Goldberg and P. Nienow (2015), Modeling the impact of glacial runoff on fjord circulation and submarine melt rate using a new subgrid-scale parameterization for glacial plumes, *J. Geophys. Res. Oceans*, 120, 796–812, https://doi.org/10.1002/2014JC010324.

Davison, B. J., T. Cowton, A. Sole, F. Cottier and P. Nienow (2022), Modelling the effect of submarine iceberg melting on glacier-adjacent water properties, *The Cryosphere*, 16, 1181–1196, https://doi.org/10.5194/tc-16-1181-2022.

Davison, B. J., T. R. Cowton, F. R. Cottier and A. J. Sole (2020), Iceberg melting substantially modifies oceanic heat flux towards a major Greenlandic tidewater glacier, *Nat. Commun.*, 11, 5983, https://doi.org/10.1038/s41467-020-19805-7.

De Andrés, E., J. Otero, F. Navarro, A. Promińska, J. Lapazaran and W. Walczowski (2018), A two-dimensional glacier–fjord coupled model applied to estimate submarine melt rates and front position changes of Hansbreen, Svalbard, *J. Glaciol.*, 64, 745–758, https://doi.org/10.1017/jog.2018.61.

De Andrés, E., D. A. Slater, F. Straneo, J. Otero, S. Das and F. Navarro (2020), Surface emergence of glacial plumes determined by fjord stratification, *The Cryosphere*, 14(6), 1951–1969, https://doi.org/10.5194/tc-14-1951-2020.

Enderlin, E. M., C. J. Carrigan, W. H. Kochtitzky, A. Cuadros, T. Moon and G. S. Hamilton (2018), Greenland iceberg melt variability from high-resolution satellite observations, *The Cryosphere*, 12, 565–575, https://doi.org/10.5194/tc-12-565-2018.

Enderlin, E. M., G. S. Hamilton, F. Straneo and D. A. Sutherland (2016), Iceberg meltwater fluxes dominate the freshwater budget in Greenland's iceberg-congested glacial fjords, *Geophys. Res. Lett.*, 43, 11287–11294, https://doi.org/10.1002/2016GL070718.

FitzMaurice, A., C. Cenedese and F. Straneo (2017), Nonlinear response of iceberg side melting to ocean currents, *Geophys. Res. Lett.*, 44, 5637–5644, https://doi.org/10.1002/2017GL073585.

Fraser, N. J., M. E. Inall, M. G. Magaldi, T. W. N. Haine and S. C. Jones (2018), Wintertime fjord-shelf interaction and ice sheet melting in Southeast Greenland, *J. Geophys. Res. Oceans*, 123, 9156–9177, https://doi.org/10.1029/2018JC014435.

Gade, H. G. (1979), Melting of ice in sea water: A primitive model with application to the antarctic ice shelf and icebergs, *J. Phys. Oceanogr.*, 9, 189–198, https://doi.org/10.1175/1520-0485(1979)009<0189:MOIISW>2.0.CO;2.

Gladish, C. V., D. M. Holland, A. Rosing-Asvid, J. W. Behrens and J. Boje (2015), Oceanic boundary conditions for Jakobshavn Glacier. Part I: Variability and renewal of Ilulissat Icefjord waters, 2001–14, *J. Phys. Oceanogr.*, 45, 3–32, https://doi.org/10.1175/JPO-D-14-0044.1.

Greisman, P. (1979), On upwelling driven by the melt of ice shelves and tidewater glaciers, *Deep Sea Res. A*, 26, 1051–1065, https://doi.org/10.1016/0198-0149(79)90047-5.

Hager, A. O., D. A. Sutherland, J. M. Amundson, R. H. Jackson, C. Kienholz, R. J. Motyka and J. D. Nash (2022), Subglacial discharge reflux and buoyancy forcing drive seasonality in a silled glacial fjord, *J. Geophys. Res. Oceans*, 127, https://doi.org/10.1029/2021JC018355.

Hermann, A. J., P. B. Rhines and E. R. Johnson (1989), Nonlinear Rossby adjustment in a channel: beyond Kelvin waves, *J. Fluid Mech.*, 205, 469–502, https://doi.org/10.1017/S0022112089002119.

Hester, E. W., C. D. McConnochie, C. Cenedese, L.-A. Couston and G. Vasil (2021), Aspect ratio affects iceberg melting, *Phys. Rev. Fluids*, 6, 023802, https://doi.org/10.1103/PhysRevFluids.6.023802.

Hughes, K. G. (2022), Pathways, form drag, and turbulence in simulations of an ocean flowing through an ice mélange, *J. Geophys. Res. Oceans*, 127, e2021JC018228, https://doi.org/10.1029/2021JC018228.

Inall, M. E., T. Murray, F. R. Cottier, K. Scharrer, T. J. Boyd, K. J. Heywood and S. L. Bevan (2014), Oceanic heat delivery via Kangerdlugssuaq Fjord to the south-east Greenland ice sheet, *J. Geophys. Res. Oceans*, 119, 631–645, https://doi.org/10.1002/2013JC009295.

Jackson, R. H., R. J. Motyka, J. M. Amundson, N. Abib, D. A. Sutherland, J. D. Nash and C. Kienholz (2022), The relationship between submarine melt and subglacial discharge from observations at a tidewater glacier, *J. Geophys. Res. Oceans*, 127, e2021JC018204, https://doi.org/10.1029/2021JC018204.

Jackson, R. H., J. D. Nash, C. Kienholz, D. A. Sutherland, J. M. Amundson, R. J. Motyka, D. Winters, E. Skyllingstad and E. C. Pettit (2020), Meltwater intrusions reveal mechanisms for rapid submarine melt at a tidewater glacier, *Geophys. Res. Lett.*, 47, e2019GL085335, https://doi.org/10.1029/2019GL085335.

Jackson, R. H., E. L. Shroyer, J. D. Nash, D. A. Sutherland, D. Carroll, M. J. Fried, G. A. Catania, T. C. Bartholomaus and L. A. Stearns (2017), Near-glacier surveying of a subglacial discharge plume: Implications for plume parameterizations, *Geophys. Res. Lett.*, 44, 6886–6894, https://doi.org/10.1002/2017GL073602.

Jackson, R. H. and F. Straneo (2016), Heat, salt, and freshwater budgets for a glacial fjord in Greenland, *J. Phys. Oceanogr.*, 46, 2735–2768, https://doi.org/10.1175/JPO-D-15-0134.1.

Jenkins, A. (2011), Convection-driven melting near the grounding lines of ice shelves and tidewater glaciers, *J. Phys. Oceanogr.*, 41, 2279–2294, https://doi.org/10.1175/JPO-D-11-03.1.

Josberger, E. G. and S. Neshyba (1980), Iceberg melt-driven convection inferred from field measurements of temperature, *Ann. Glaciol.*, 1, 113–117, https://doi.org/10.3189/S0260305500017080.

Klymak, J. M. and S. M. Legg (2010), A simple mixing scheme for models that resolve breaking internal waves, *Ocean Modell.*, 33, 224–234, https://doi.org/10.1016/j.ocemod.2010.02.005.

Kopera, M., Y. Gahounzo, E. M. Enderlin and F. X. Giraldo (2022), Non-hydrostatic unified model of the ocean with application to ice/ocean interaction modeling, https://doi.org/10.13140/RG.2.2.35929.80488.

Losch, M. (2008), Modeling ice shelf cavities in a z coordinate ocean general circulation model, *J. Geophys. Res.*, 113, C08043, https://doi.org/10.1029/2007JC004368.

Magorrian, S. J. and A. J. Wells (2016), Turbulent plumes from a glacier terminus melting in a stratified ocean, *J. Geophys. Res. Oceans*, 121, 4670–4696, https://doi.org/10.1002/2015JC011160.

Malyarenko, A., A. J. Wells, P. J. Langhorne, N. J. Robinson, M. J. Williams and K. W. Nicholls (2020), A synthesis of thermodynamic ablation at ice–ocean interfaces from theory, observations and models, *Ocean Modell.*, 154, 101692, https://doi.org/10.1016/j.ocemod.2020.101692.

Marshall, J., A. Adcroft, C. Hill, L. Perelman and C. Heisey (1997), A finite-volume, incompressible Navier Stokes model for studies of the ocean on parallel computers, *J. Geophys. Res.*, 102, 5753–5766, https://doi.org/10.1029/96JC02775.

Melton, S. M., R. B. Alley, S. Anandakrishnan, B. R. Parizek, M. G. Shahin, L. A. Stearns, A. L. LeWinter and D. C. Finnegan (2022), Meltwater drainage and iceberg calving observed in high-spatiotemporal resolution at Helheim Glacier, Greenland, *J. of Glaciology*, 68(270), 812–828, https://doi.org/10.1017/jog.2021.141.

Moon, T., D. A. Sutherland, D. Carroll, D. Felikson, L. Kehrl and F. Straneo (2018), Subsurface iceberg melt key to Greenland fjord freshwater budget, *Nat. Geosci.*, 11, 49–54, https://doi.org/10.1038/s41561-017-0018-z.

Mortensen, J., S. Rysgaard, J. Bendtsen, K. Lennert, T. Kanzow, H. Lund and L. Meire (2020), Subglacial discharge and its down-fjord transformation in West Greenland fjords with an ice mélange, *J. Geophys. Res. Oceans*, 125, e2020JC016301, https://doi.org/10.1029/2020JC016301.

Moyer, A. N., D. A. Sutherland, P. W. Nienow and A. J. Sole (2019), Seasonal variations in iceberg freshwater flux in Sermilik Fjord, Southeast Greenland from Sentinel-2 imagery, *Geophys. Res. Lett.*, 46, 8903–8912, https://doi.org/10.1029/2019GL082309.

Rezvanbehbahani, S., L. A. Stearns, R. Keramati, S. Shankar and C. J. van der Veen (2020), Significant contribution of small icebergs to the freshwater budget in Greenland fjords, *Commun. Earth Environ.*, 1, 31, https://doi.org/10.1038/s43247-020-00032-3.

Schulz, K., A. T. Nguyen and H. R. Pillar (2022), An improved and observationally-constrained melt rate parameterization for vertical ice fronts of marine terminating glaciers, *Geophys. Res. Lett.*, 49, e2022GL100654, https://doi.org/10.1029/2022GL100654.

Sciascia, R., F. Straneo, C. Cenedese and P. Heimbach (2013), Seasonal variability of submarine melt rate and circulation in an East Greenland fjord, *J. Geophys. Res. Oceans*, 118, 2492–2506, https://doi.org/10.1002/jgrc.20142.

Shin, H. H., D. Muñoz-Esparza, J. A. Sauer and M. Steiner (2021), Large-eddy simulations of stability-varying atmospheric boundary layer flow over isolated buildings, *J. Atmos. Sci.*, 78, 1487–1501, https://doi.org/10.1175/JAS-D-20-0160.1.

Slater, D. A., D. Carroll, H. Oliver, M. J. Hopwood, F. Straneo, M. Wood, J. K. Willis and M. Morlighem (2022), Characteristic depths, fluxes, and timescales for Greenland's tidewater glacier fjords from subglacial discharge-driven upwelling during summer, *Geophys. Res. Lett.*, 49, e2021GL097081, https://doi.org/10.1029/2021GL097081.

Slater, D. A., D. N. Goldberg, P. W. Nienow and T. R. Cowton (2016), Scalings for submarine melting at tidewater glaciers from buoyant plume theory, *J. Phys. Oceanogr.*, 46, 1839–1855, https://doi.org/10.1175/JPO-D-15-0132.1.

Slater, D. A., P. W. Nienow, T. R. Cowton, D. N. Goldberg and A. J. Sole (2015), Effect of near-terminus subglacial hydrology on tidewater glacier submarine melt rates, *Geophys. Res. Lett.*, 42(8), 2861–2868, https://doi.org/10.1002/2014GL062494.

Slater, D. A., F. Straneo, S. B. Das, C. G. Richards, T. J. W. Wagner and P. W. Nienow (2018), Localized plumes drive front-wide ocean melting of a Greenlandic tidewater glacier, *Geophys. Res. Lett.*, 45, 12350–12358, https://doi.org/10.1029/2018GL080763.

Straneo, F., R. G. Curry, D. A. Sutherland, G. S. Hamilton, C. Cenedese, K. Våge and L. A. Stearns (2011), Impact of fjord dynamics and glacial runoff on the circulation near Helheim Glacier, *Nat. Geosci.*, 4, 322–327, https://doi.org/10.1038/ngeo1109.

Stuart, G. A., M. A. Sundermeyer and D. Hebert (2011), On the geostrophic adjustment of an isolated lens: Dependence on Burger number and initial geometry, *J. Phys. Oceanogr.*, 41, 725–741, https://doi.org/10.1175/2010JPO4476.1.

Sulak, D. J., D. A. Sutherland, E. M. Enderlin, L. A. Stearns and G. S. Hamilton (2017), Iceberg properties and distributions in three Greenlandic fjords using satellite imagery, *Ann. Glaciol.*, 58, 92–106, https://doi.org/10.1017/aog.2017.5.

Truffer, M. and R. J. Motyka (2016), Where glaciers meet water: Subaqueous melt and its relevance to glaciers in various settings, *Rev. Geophys.*, 54, 220–239, https://doi.org/10.1002/2015RG000494.

Wood, M., E. Rignot, I. Fenty et al. (2021), Ocean forcing drives glacier retreat in Greenland, *Sci. Adv.*, 7, eaba7282, https://doi.org/10.1126/sciadv.aba7282.

Xu, Y., E. Rignot, I. Fenty, D. Menemenlis and M. M. Flexas (2013), Subaqueous melting of Store Glacier, west Greenland from three-dimensional, high-resolution numerical modeling and ocean observations, *Geophys. Res. Lett.*, 40, 4648–4653, https://doi.org/10.1002/grl.50825.

Xu, Y., E. Rignot, D. Menemenlis and M. Koppes (2012), Numerical experiments on subaqueous melting of Greenland tidewater glaciers in response to ocean warming and enhanced subglacial discharge, *Ann. Glaciol.*, 53, 229–234, https://doi.org/10.3189/2012AoG60A139.

Yankovsky, A. E. and I. Yashayaev (2014), Surface buoyant plumes from melting icebergs in the Labrador Sea, *Deep Sea Res.*, 91, 1–9, https://doi.org/10.1016/j.dsr.2014.05.014.

Zhao, K. (2022), Standing eddies in glacial fjords and their role in fjord circulation and melt, *Earth and Space Science Open Archive*, https://doi.org/10.1002/essoar.10511100.1.

Zhao, K. X., A. L. Stewart and J. C. McWilliams (2021), Geometric constraints on glacial fjord–shelf exchange, *J. Phys. Oceanogr.*, 51, 1223–1246, https://doi.org/10.1175/JPO-D-20-0091.1.

Zhao, K. X., A. L. Stewart and J. C. McWilliams (2022), Linking overturning, recirculation, and melt in glacial fjords, *Geophys. Res. Lett.*, 49, e2021GL095706, https://doi.org/10.1029/2021GL095706.